Hindawi
Advances in Materials Science and Engineering
Volume 2017, Article ID 7967848, 12 pages
https://doi.org/10.1155/2017/7967848

Research Article

Synthesis and Characterization of Zn-Ni$_x$ Advanced Alloys Prepared by Mechanical Milling and Sintering at Solid-State Process

José G. Miranda-Hernández,[1] Héctor Herrera-Hernández,[1] Carlos O. González-Morán,[1] Jesús Noé Rivera Olvera,[2] Ivanovich Estrada-Guel,[3] and Fabián Botello Villa[1]

[1]*Universidad Autónoma del Estado de México, Centro Universitario UAEM Valle de México, Laboratorio de Investigación y Desarrollo de Materiales Industriales, 54500 Atizapán de Zaragoza, MEX, Mexico*
[2]*Tecnológico de Estudios Superiores de Ixtapaluca, 56580 Ixtapaluca, MEX, Mexico*
[3]*Centro de Investigación en Materiales Avanzados (CIMAV), Laboratorio Nacional de Nanotecnología, 31136 Chihuahua, CHIH, Mexico*

Correspondence should be addressed to Héctor Herrera-Hernández; hherrerah@uaemex.mx

Received 2 July 2017; Revised 3 October 2017; Accepted 12 October 2017; Published 28 December 2017

Academic Editor: Andres Sotelo

Mechanical ball milling assisted by sintering in the solid state was used in this research to produce the Zn-Ni$_x$ system alloy. The derivative powder compositions of Zn-Ni$_x$ ($x = 0$, 5, 10, 15, and 20 wt.%) were obtained to study the Ni effects on the microstructural and mechanical properties. It is worth remarking that conventional methods are not appropriate for the manufacture of the Zn-Ni$_x$ system alloy. The morphological structure and phases were examined by optical microscopy, X-ray diffraction, and SEM/EDS elemental mapping, whereas the mechanical behavior was accomplished by means of a diamond indentation print (Hardness Vickers). The results showed that the intermetallic γ-ZnNi phase did not form during milling time (<4 h); it appears after the sintering process, which is associated with atomic diffusion mechanism through grain boundary at the minimum interfacial energy ($\Delta G256^{\circ}C = -13.83\ kJ{\cdot}mol^{-1}$). The powder Zn-Ni$_{10}$ was found to have better properties. Semispherical coarser particles were seen into the metal matrix (Zn δ-hcp structure) as segregates; however, each particle contains an intermetallic compound Zn-Ni that encloses the Ni (α-fcc structure) pure phase. The Ni-α phase was then transformed into a γ-ZnNi intermetallic compound which shifts to higher values of mechanical hardness from about 60 HV to 400 HV units.

1. Introduction

In the last days, the study of the physical and chemical properties of metals and their alloys has led to develop new manufacturing technologies for high-quality applications, in which the metallic materials are involved [1]. However, in the last quarter of the twentieth century, there has been an advancement in the characterization, analysis, and processing of metallic materials, having allowed the development of new advanced alloys. There are several systems of metal mixtures such as nickel (Ni) base alloys in which the interest lies in their higher corrosion resistance, which is commonly used in oil- and chemical-processing industries, and for a long time, zinc (Zn) alloys have primarily been studied because of their light weight and good corrosion resistance and recently have been used as metal coatings to provide any type of surface protection for automobile parts or building materials [2, 3].

Most recently, considerable attention has increasingly been focused on advanced procedures in dispersing Ni atoms into Zn-matrix structure, which is one of the great interests of our research group. Therefore, there have been several studies in the literature that report the possibility of manufacturing metallic alloys and intermetallic compounds

of Zn-Ni by procedures of immersion in chloride salt baths, mechanical alloying, electrodeposition, and sintered and sol-gel treatments, in which these studies were based on the analysis of the microstructural changes, catalytic activity, mechanical behavior, and thermodynamic and electrical properties [2, 4–14]. Other studies, like Sn-9%Zn alloy, show that the addition of other chemical elements has some effects on the microstructural, thermal, and mechanical properties [15], and this behavior is also seen in metal matrix composites (MMCs) [16–18]. However, several studies are related to the use of the high-energy mechanical milling (HEMM) also known as mechanical alloying (MA). MA technology has been used almost 60 years as an alternative processing of various materials such as metal powder alloys, composites, intermetallic compounds, casting alloys, and ceramics [8, 19–21]. It is important to consider that MA is a milling process at high energy in dry or wet conditions in order to produce metallic powders or metal matrix composites giving unique properties by controlling the microstructure. This can be possible by successive fracture and welding mechanism of a powder mixture containing metallic particles (as a reinforcing material) under high-energy impact of steel balls, known as mechanical grinding media.

Other researchers have reported that, by controlling the variables of milling time, grinding media, and their rotational speed in rpm, a nanostructured alloy with advanced and unique properties is obtained. Unique conditions are the great attractive interest for researchers due to the control of the microstructure during the synthesis of materials by mechanical milling, whose purpose is to obtain desired physical and mechanical properties such as low density, uniform microporosity, good hardness and fracture toughness, and high Young's modulus, among other properties [6, 9, 20–24]. In turn, the effects of Ni addition in the binary Zn base alloy are of great interest to study in this research, by considering the mechanical milling at high energy as a nonequilibrium method and the consolidation of the material by sintering process in the solid state as the only alternative to produce materials with high performance and unique properties that cannot be obtained by conventional manufacturing procedures because of the melting temperature differences. Therefore, this study comprises two fundamental interests: the first one realized in this work is to evaluate the microstructural characteristics and the effect on mechanical behavior of Ni particles in the metal alloy and the second as a future work is to evaluate the electrocatalytic viability as a sustainable material for its possible application of energy cells due to the hydrogen evolution reaction (HER). There is in the literature information related to using Ni base alloys for that kind of application [25–30].

2. Experimental Procedure

The powder Zn-Ni_x alloy system (Zn-Ni_5, Zn-Ni_{10}, Zn-Ni_{15}, and Zn-Ni_{20}) was manufactured using the solid-state sintering process assisted by mechanically milling alloys at high energy. Commercially finer powders of high purity at reagent grade were used in this research as raw materials (99.00% of pure zinc powder (mesh #200, J. T. Baker) and 99.90% of pure nickel powder (mesh #100, Meyer)). 10 g of raw materials (initial powders) were weighed and mixed in a ceramic container to form stoichiometric binary composition-based Zn at different Ni contents ($x = 0$, 5, 10, 15, and 20 wt.%). Therefore, the powder mixtures were immediately placed into a cylindrical 250 ml container of agate (SiO_2) and were subjected to a process of mechanical milling using a planetary high-energy ball mill ("FRITSCH" model Pulverisette 6) at 200 rpm rotating speed for 4 hours. After milling, a total of 9.2 g of sample was recovered, and after sintering, 9.1 g was recovered. Thus, the milling conditions were determined, according to our previous experience. Agate balls of 10 mm diameter were also introduced in the system as grinding media. The ratio of powder to balls used was 10 : 1 in wet condition, for which purpose, 20% by volume of isopropyl alcohol (C_3H_7OH) was added as a controlling process agent to homogenize the mixture and prevent the metal particle agglomeration or cold welding. Subsequently, the powder mixtures were uniaxially compacted into a cylindrical form (20 mm diameter and 2 mm thickness, size of the metal die) by applying a total load of 300 MPa at room temperature, and no additives were used. The compacted powder samples were then consolidated by a solid-state sintering treatment at a heating rate of 10°C/min using an electric furnace at 357°C for one hour under a controlled atmosphere of nitrogen gas, followed by slow cooling in the furnace. Prior to reach the maximum temperature (357°C), a heating ramp at 250°C for 30 minutes is applied. This thermal procedure is shown in Figure 1.

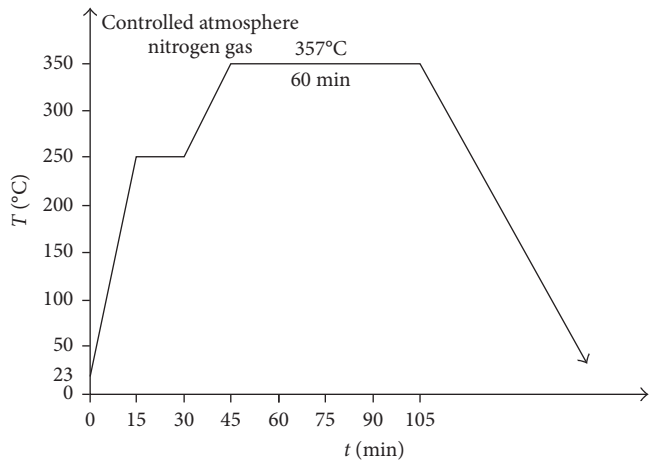

Figure 1: Sequence of the thermal treatment applied to the compacted Zn-Ni_x powders for their densification in the solid state.

The relative density and apparent porosity of the sintered powders were determined according to Archimedes' principle at room temperature. The surface of sintered compacts was prepared by means of standard metallographic procedures. Immediately, the corresponding microstructure was examined by using an OLYMPUS GX51 optical microscope and a JEOL JSM6300 scanning electron microscope (SEM) equipped with an energy-dispersive X-ray spectroscopy (EDS) detector, which was used to analyze the elemental contents (mapping) operating with an

Table 1: Comparison of the theoretical and experimental densities of Zn-Ni$_x$ metal compounds.

System Zn-Ni$_x$	Zn	Zn-Ni$_5$	Zn-Ni$_{10}$	Zn-Ni$_{15}$	Zn-Ni$_{20}$
ρ_t (g/cm^3)	7.13	7.22	7.31	7.40	7.48
ρ_e (g/cm^3)	6.51	6.52	6.54	6.57	6.61

acceleration voltage of 15 kV applied to the working distance (WD) of 7.2 mm. X-ray diffraction (XRD) analysis of the samples was performed in a BRUKER D8 ADVANCE diffractometer, using Kα of Cu monochromatic radiation ($\lambda = 1.5406$ Å) at a scan rate of 4°C/min in order to identify the crystalline phases existent in the powder mixture alloy. The microhardness was determined as a measure of mechanical properties using the Vickers indentation test (model DURASCAN-20) according to ASTM: B 933-09. An indentation load of 0.245 N was applied for 10 s on samples prepared by metallography techniques. Finally, elementary nickel or zinc base metal powder samples were also prepared for comparison purposes.

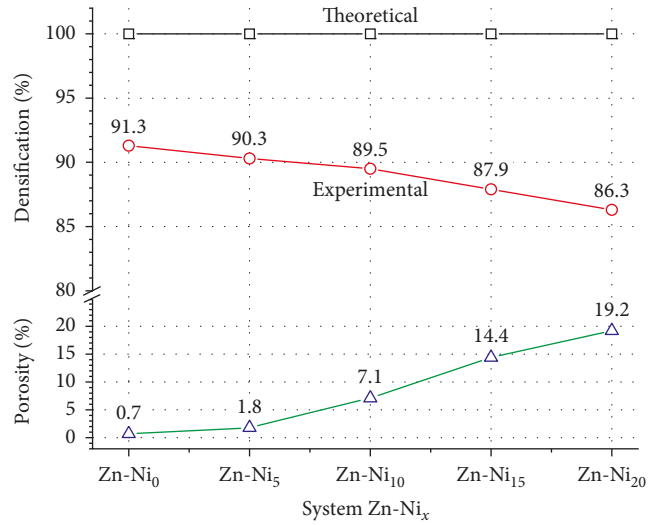

Figure 2: Densification behavior and porosity from powder alloys of Zn-Ni$_x$.

3. Results and Discussion

3.1. Relative Density and Porosity Measurements. The relative density of the green compacted Zn-Ni$_5$ powder alloy resulted to be about 6.20 g/cm^3, which increases slightly to 6.52 g/cm^3 when the compacts are subjected to a sintering process, so that the alloy during the heat treatment undergoes a volumetric contraction of 0.45%, and this treatment also decreases the percentage of apparent porosity from 18.2% to 1.8%. These results indicate that sintered samples exhibited the greater density than that observed on green compacted samples after pressing at 300 MPa, which is associated with the presence of interconnected pores in the green body structure, where the pores are not completely eliminated during the plastic deformation mechanism of the Zn base alloy that happens in isostatic cold pressing. It is possible to comment that the contraction percentage of the alloy is relatively lower. Table 1 shows the result of the experimental density (ρ_e) obtained for the Zn-Ni$_x$ alloy system (x denotes Ni composition at 0, 5, 10, 15, and 20 wt.%, resp.) after the sintering process, and a comparison with its respective theoretical density (ρ_t) was also showed. In addition, the porosity can also be associated with the milling process as is explained in the literature [31]. They reported from the BET results that the surface area of the samples is strongly dependent on the mechanical milling method [31]. This means that the porosity can be due to a decrease in the crystal size as a function of the transformation of elemental powders by the mechanical deformation of the powder particle and an increase in the defect density. Table 1 also includes pure Zn. The results indicate that the theoretical density and the experimental density increase slightly with an increase in Ni content in the alloy. This is probably associated with the addition of a dense component (Ni = 8.90 g/cm^3) into the structural system of Zn-Ni$_x$.

The plot in Figure 2 shows the percentage relationship of porosity and densification of the powder materials after being sintered. The pure Zn used as a reference material resulted to have the lowest porosity of about 0.7% compared with the rest of the manufactured compounds of the Zn-Ni$_x$ system. While the Zn-Ni$_{20}$ alloy has the highest porosity percentage of about 19.2%, this condition indicates that a higher addition of Ni wt.% in the alloy increases the presence of pores in the bulk material. This fact could be attributed to the phenomenon of activation energy "atomic diffusion that takes place during the sintering process." In agreement with the Hume-Rothery rule, the substitutional solution occurs when the relative difference between the atomic radii of the two species is less than 15%. The atomic radii of Zn and Ni are 0.139 nm and 0.200 nm, respectively, and the atomic size factor is 30.5% (>15%), which indicates that a substitutional solubility between Zn and Ni is not possible. In addition, the ratio of the radius of the interstitial atom to the radius of the atom must be less than 0.59 for the formation of an interstitial phase [32]. The atomic radii ratio between Zn and Ni is approximately 0.695 (>0.59), which indicates that the nickel atomic radii are too small to accommodate the zinc in the interstitial position.

These results can be possibly explained by the diffusion of Zn or Ni particles in the alloy matrix, which contributes in filling up the pores through Zn-Ni and Ni-Ni particle interactions. Accordingly, the well-known binary phase diagram of Ni-Zn [27, 28] (illustrated in Figure 3) shows a large ratio of melting points between the Zn matrix (~419.5°C) and the reinforcement Ni-phase particles (~1455°C). This allows to have a considerable driving force, that promotes the atomic mobility mechanism at the solid state in order to increase the interaction between Ni-Zn and Zn-Zn particles; in this sense, thermodynamically, this binary system contains a liquid phase, intermetallic compounds such as β, β_1, and γ, and equilibrium phases like α (Ni-fcc structure) and δ (Zn-hcp structure). However, at the temperature of about 357°C in which the process of sintering occurs, Ni atoms

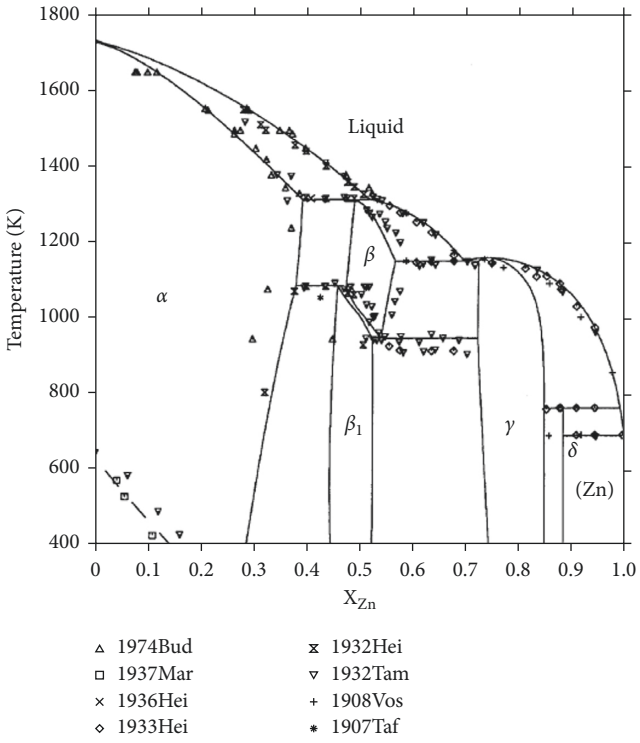

Figure 3: An equilibrium Ni-Zn phase diagram thermodynamically calculated by Su et al. [33].

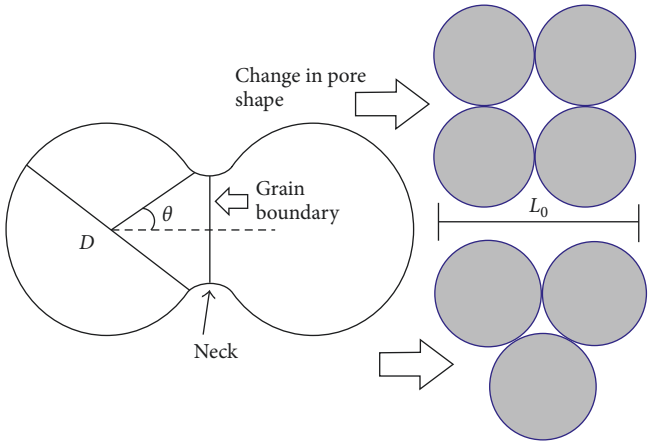

Figure 4: Mechanism of the sintering process. Necking stage formation between particles and their growth and porosity distribution. D is the particle diameter, θ is the diffusion angle, and L_0 is the initial distance of particles.

diffuse very slowly into the Zn structure; this could be attributed to the fact of having large differences in melting temperatures [34]. It is worth noting to comment that the sintering process improves the density of the green powder compacts. This mechanism is indicated in the sintered model illustrated in Figure 4.

The bonding of Zn-Ni powder particles requires a driving force ($T < T_f$) to facilitate the mass transport mechanism from the interior of the particles to the contact points with one another, so sintering is driven by the desire to minimize the free surface energy ($\Delta G_{\text{surface}} < 0$) of the agglomerate particles to create necks between the spherical particles which then leads to fusion of particles. It is assumed that only spherical particles can change their shape during densification. This indicates that the centers of the particles are approaching and the volume of the sample will decrease. So, the superficial area leads to produce grain boundaries GB (γ), and the interfacial energy (γGB) of GB results in less energy than in the two surface areas; energy that is released during the grain boundary formation; in this sense, the total free energy of the Zn-Ni_x system is reduced. It is also noticed that the mass transport mechanism in the Zn-Ni_x system is possible during the sintering process. This could be happened by (i) volume diffusion or (ii) grain boundary diffusion. With the advance of the sintering is possible to reach the theoretical density of near 90%; at this stage, shrinkage and close pores are homogeneously well distributed in the structure of the alloy.

According to the Zn-Ni phase diagram that is shown in Figure 3, the percentage composition of the study systems ranges from 0% < Ni < 15%, and an intermetallic phase δ is presented, while in the range of 15% < Ni < 20%, the intermetallic phase changes to γ; however, considering that the limit of 15% can have the presence of both phases, according to this diagram, there is not any chance of possibility of finding intermetallic phases of β and β_1. It is important to note that, according to the XRD spectra of the systems Zn-Ni_5, Zn-Ni_{10}, Zn-Ni_{15}, and Zn-Ni_{20} during high-energy milling, no formation of intermetallic phases was identified, whereas the main mechanism for the formation of these kinds of phases is by increasing the energy during the impact between the grinding media and powders to enable the diffusion and promote the reaction of formation of the intermetallic compound. In the particular case of these systems and due to the manufacturing methodology proposed in this research, high-energy milling is just a mix-milling process that homogenizes the composition of the systems. In this sense, some systems do not present the formation of these compounds by mechanical action due to insufficient energy transfer to the powder but obtained after a heating process.

On the other hand, Figure 2 also shows a gradual decrease in the densification of the Zn matrix as a function of Ni addition. This could be explained by the differences in the atomic radius that produces a structural distortion leaving more pores and defects, according to the model in Figure 4. The pure Zn as a reference sample reached a densification of about 91.3%. The compound Zn-Ni_5 has a densification of 90.3%, while the Zn-Ni_{10} showed a density of 89.5% in this trend. This indicates that the less dense material was for the compound Zn-Ni_{20}, which has a densification of 86.3%. This behavior is directly related to the increasing Ni addition (wt.%) and is inversely proportional to the porosity. In this sense, it is possible to mention that the sintering process at the solid state plays an important role in densification, and its contribution results in the minimization of interfacial activation energy for diffusion to occur, and also the shape of powders particles (i.e., spherical) has a strong influence on

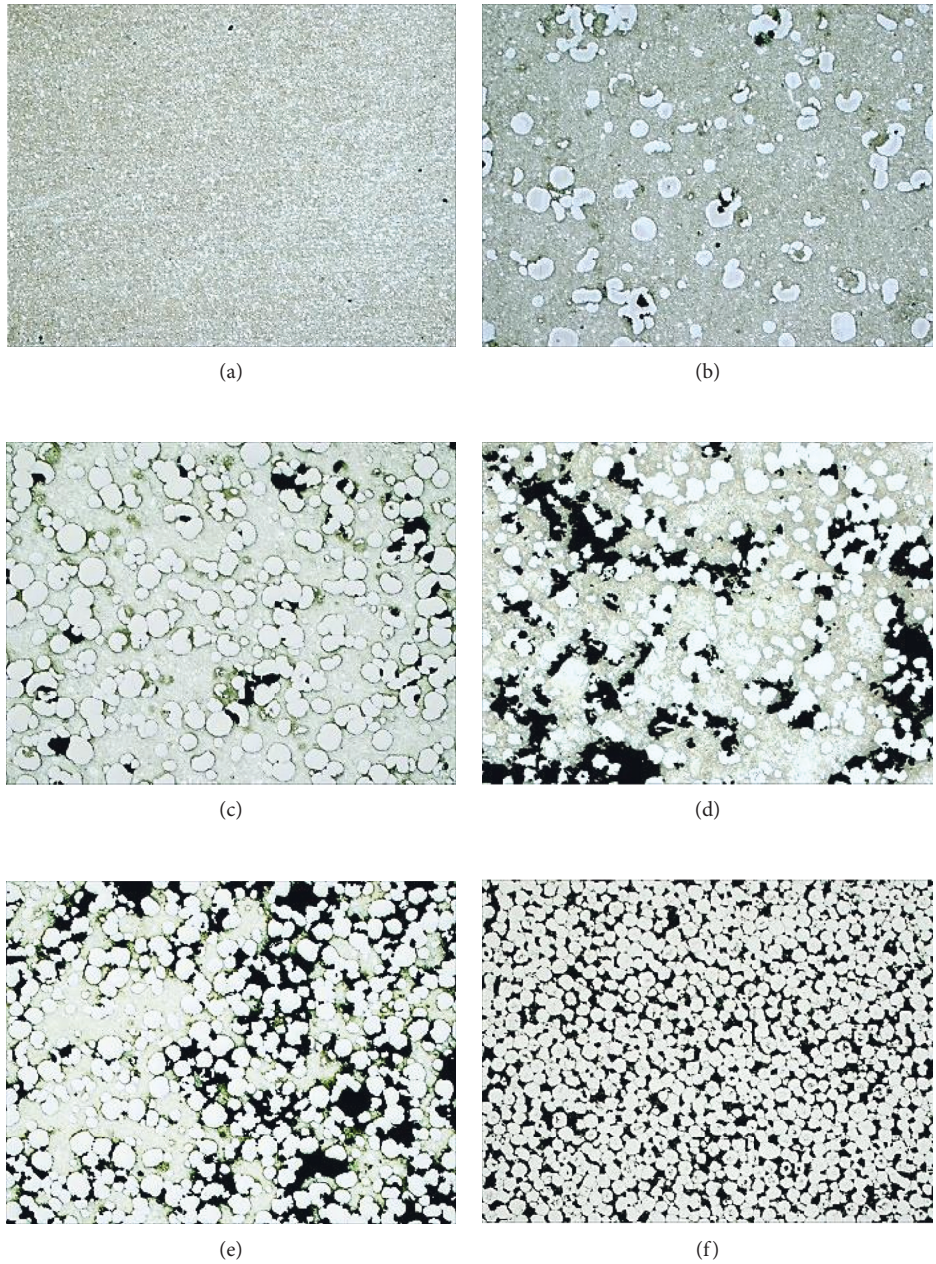

Figure 5: Optical microstructures obtained at 5x of the system Zn-Ni$_x$: (a) Zn, (b) Zn-Ni$_5$, (c) Zn-Ni$_{10}$, (d) Zn-Ni$_{15}$, (e) Zn-Ni$_{20}$, and (f) Ni.

sintering behavior, as well as on Ni addition. So, the authors suggest that sintering is an important process that has an impact on the final properties of the manufactured advanced materials in their industrial application.

3.2. Microstructure. The microstructural modification during the synthesis of the Zn-Ni$_x$ powder system alloy by nonconventional procedures (i.e., high-energy mechanical milling) is based on the concept of phase transformation that occurs by the diffusion phenomena at the solid state. This feature is clearly seen in the microstructures shown in Figure 5. The typical microstructures of the Zn-Ni$_x$ binary system at different compositions obtained are depicted in Figure 5, from which it can be seen that porosity is distributed along the bulk of Zn matrix that increased as Ni addition increased, and it is possible to note that porosity directly affects the densification of the Zn-Ni powder alloy.

The microstructures corresponding to the compositions Zn-Ni$_5$, Zn-Ni$_{10}$, Zn-Ni$_{15}$, and Zn-Ni$_{20}$ are seen in Figures 5(b)–5(e), from which some details are expected: (i) coarser precipitates (light-gray phase) with a semispherical shape are observed on the Zn matrix, that possibly corresponds to the Ni phase, and it is more noticeable when the composition of this component increases. (ii) A second phase is also seen that evidently corresponds to Zn precipitates, and it is the metal matrix of the base material. (iii) Closed microporosity is only observed for the sintered Zn and Zn-Ni$_5$ powder

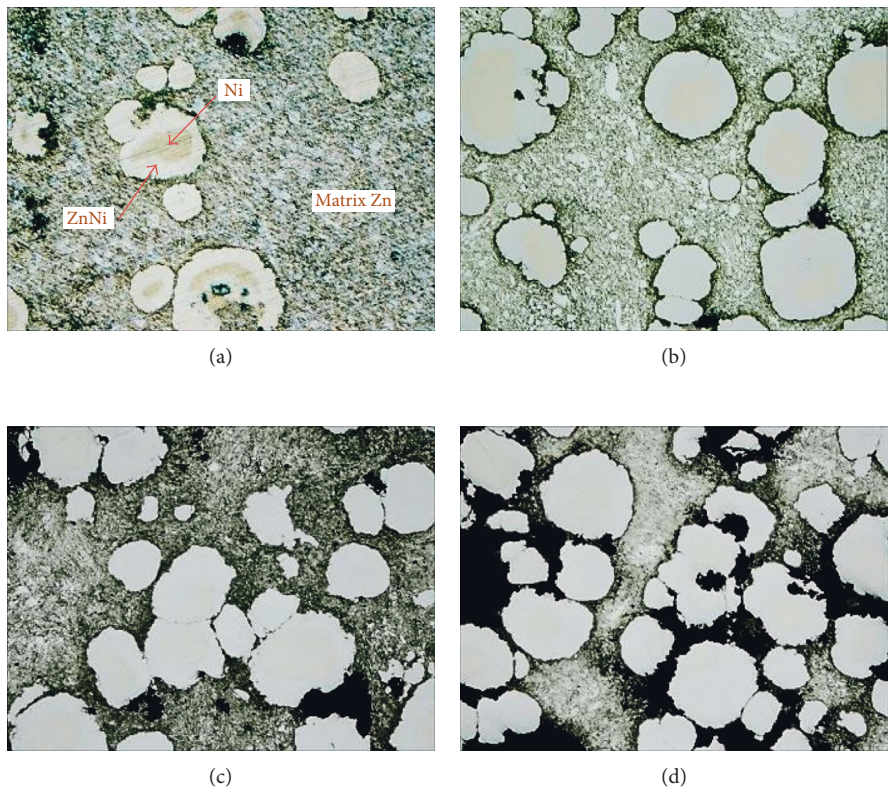

FIGURE 6: Microstructures obtained by optical microscopy at 20x of the Zn-Ni_x powder alloy system: (a) Zn-Ni_5, (b) Zn-Ni_{10}, (c) Zn-Ni_{15}, and (d) Zn-Ni_{20}.

alloys, and this fact is attributed to the rapid diffusion of Zn at the temperature of 357°C (T_s), which is very close to the melting temperature of the Zn (T_f-Zn = 419.53°C). Whereas, for the case of the sintered compounds Zn-Ni_{10}, Zn-Ni_{15}, and Zn-Ni_{20}, larger cavities were denoted on the microstructure, and these are more evident as Ni content in the alloy increases. This is due to larger differences between the melting temperature of Ni (T_f-Ni = 1455°C) and the sintering temperature (T_s) that makes Ni to diffuse slowly leaving more structural defects, as that shown in the sintered model in Figure 4. Generally speaking, the microstructural changes of the compounds after being sintered are remarkable, and it is also compared with the microstructure corresponding to pure Zn (Figure 5(a)) or pure Ni (Figure 5(f)), respectively.

Figure 6 shows the microstructures corresponding to Zn-Ni_5, Zn-Ni_{10}, Zn-Ni_{15}, and Zn-Ni_{20} obtained at 20x magnification. In these micrographs, a third phase can be seen, which presumably corresponds to an alloyed intermetallic compound formed after the sintering process at the solid state. A close inspection by optical microscopic analysis reveals that this intermetallic compound (Zn-Ni) encloses the Ni phase and it segregated homogeneously into Zn matrix, as it is shown only for the Zn-Ni_5 powder alloy (Figure 6(a)). This assumption is due to the interfacial diffusion mechanism of Ni into Zn based alloy, and no insulation of the material was observed for Zn-Ni_{15} or Zn-Ni_{20}. This behavior is not unexpected, and isolation of Ni phases has been seen only in Zn-rich alloys [35].

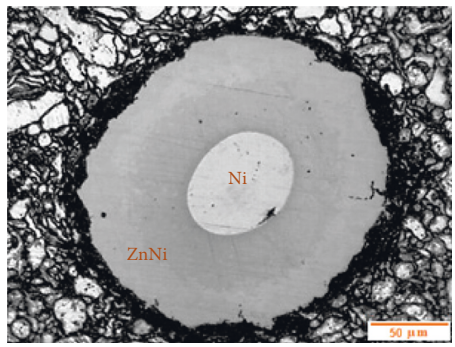

FIGURE 7: Optical microstructure of the Zn-Ni_{10} sintered powder alloy obtained at 50x, showing Zn-Ni intermetallic phase.

Figure 7 shows a semispherical particle, which shows the microstructure details of the Zn-Ni_{10} sintered powder alloy that was revealed at 50x magnification by means of optical microscopy. In this microstructure is observed that *e* and Ni phase are surrounded by the supposed Zn-Ni intermetallic compound. In addition to this, the presence of micropores is also noticed, and the Zn phase corresponds to the rest of the bulk material. In general, this microstructural behavior is only possible to be distinguished at higher magnifications (over 50x) for all the studied compositions of the system Zn-Ni_x after being sintered at the solid-state process. Based on this observation, it is assumed that the intermetallic Zn-Ni phase grows during the sintering process on preexisting sites, in which the interfacial energy is the

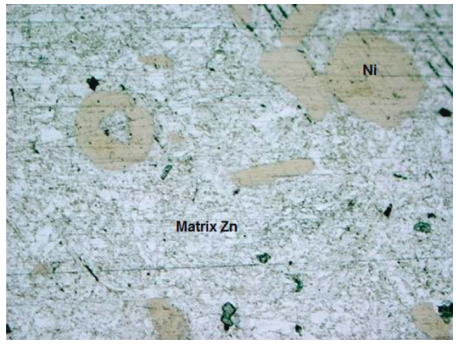

Figure 8: Typical microstructure of green compact powder obtained by optical microscopy at 20x of the Zn-Ni_5 alloy prepared by high-energy mechanical milling without sintering.

minimum for nucleation and growth mechanism, instead of forming during mechanical milling of the powder alloy. Figure 8 shows an optical microstructure of the Zn-Ni_5 powder alloy (compacted samples in a cylindrical form) without sintering; it is notable that the intermetallic phase is not present at these manufacturing conditions. So, the powder particle exhibits typically a microstructure characteristic of the mechanical milling process, which is described by spherical shape with a homogeneous distribution of the components. Also, diverse Zn-Ni_x compositions (varying Ni contents) were produced, and Ni-α-phase segregation occurs during the sintering treatment followed immediately by the α-phase growth. In this sense, the same effect was observed for all the compounds of the Zn-N_x system as that seen in the microstructures in Figure 6. After the milling condition, this micrograph is composed by Zn as the main phase (matrix) and Ni as the disperse reinforcing α-phase; however, there is not enough evidence of a possible insulation of the Zn-Ni phase as it appears in Figures 6 and 7, as is the case of sintered samples.

According to the surface examination by optical microscopy, the microstructure details of the alloy were observed, even the phase morphology and the microporosity. It can be assumed that the morphology shown in the microstructures in Figure 6 is a typical characteristic of alloys obtained by mechanical milling at high energy, in which the porosity plays an important role that considers time variables and temperature of sinter treatment [19, 22, 36]. By means of scanning electron microscopy (SEM), energy dispersive X-ray spectroscopy (EDS), and X-ray diffraction (XRD) analysis, it could be possible to identify with accuracy the phases present in the microstructure of all the compounds that comprise the Zn-Ni_x system alloy. Figure 9 shows the microstructural analysis by SEM for two compounds that correspond to Zn-Ni_5 and Zn-Ni_{10}, respectively (considering a similar response to the other compounds of the Zn-Ni_x system), and also an elemental mapping by X-ray fluorescence of the samples is shown in the same figure. This analysis by the elemental mapping could identify and determine the Ni phase (dark-gray areas) that corresponds to the isolated phase surrounded by the supposed Zn-Ni phase (light-gray areas), as that noted in the microstructures in Figures 9(a) and 9(d), so Ni was then identified as blue dots segregated and finely dispersed throughout the entire Zn matrix according to the images in Figures 9(b) and 9(e). X-ray elemental maps also identify the presence of the Zn phase as fine green dots homogeneously distributed in the digital images in Figures 9(c) and 9(f), which corresponds to Zn-Ni_5 and Zn-Ni_{10}, respectively.

An elemental composition by SEM-EDS analysis was conducted on three different regions in a localized area of the micrograph shown in Figure 10, which corresponds to the Zn-Ni_{10} compound. This figure shows the microstructure of Zn-Ni_{10} with its corresponding localized EDS spectra of the 3 selected areas. Zone 1 corresponds to the central isolated phase (dark-gray region), which is identified with higher intensity of characteristic Ni-Kα peaks; while zone 2 consists of alternated Kα peaks of Zn and Ni (light-gray region), EDS cannot identify the intermetallic compound (Zn-Ni). Zone 3 was identified as the metal matrix of Zn. According to the EDS spectra, it is possible to write the first conclusion about the formation of intermetallic compounds like Zn-Ni phase, that can only occur during the solid-state sintering treatment at the interfacial free energy condition present in the system.

The physical phenomenon that allows the formation of this phase (Zn-Ni) is by means of atomic diffusion mechanism of Zn into Ni matrix through the grain boundary; however, it should be considered that (i) Ni has the higher melting point than that of Zn, (ii) Zn represents the principal proportion in atomic % in the powder alloy, and (iii) the relationship between the sintering temperature and melting point is about 85%, under favorable conditions to promote a more rapid diffusion of Zn at high energy to achieve a better densification of the powder alloy. But, it must be kept in mind that one of the goals of solid-state sintering is its kinetic control of the growth of the grain size and also the microstructural details resulted from the lowest sintering temperature and time. It is expected that the following Zn-Ni phase has been grown by the diffusion mechanism described above, illustrated in Figures 4 and 7.

Figure 11 shows the X-ray diffraction patterns of the milled and sintered powder samples of Zn base with 5, 10, 15, and 20% of Ni content (wt.%). The results were indexed with JCPDS cards, and the indexing lines correspond to the presence of Ni-α and Zn-δ phases, whereas the formation of the intermetallic phase (γ-ZnNi) appears after the sintering process, which is identified at preferential orientation with lower intensities. The disappearance of the intensity of Ni (111) and shift to angles of less diffraction are observed, while the most intense peak of Zn is observed in the direction (101) as that shown in Figures 11(a)–11(d), which indicate an increase in the lattice parameters that possibly is associated with a hexagonal structure Zn-δ phase. Ni-α corresponds to a cubic structure decomposition, and dissolution of its atoms during the structure transformation of Zn into the intermediate phase δ-ZnNi for 5% Ni occurred, while for the percentages of 10, 15, and 20%, Ni was transformed to the γ-ZnNi phase. Although in the experimental process, the oxidation of the powder samples was controlled by means of inert gas atmosphere, and oxygen can be diffused from the environment towards the metal powder samples during its handling. The XRD patterns show the appearance of intense lines in the planes of (100) and (002) that is

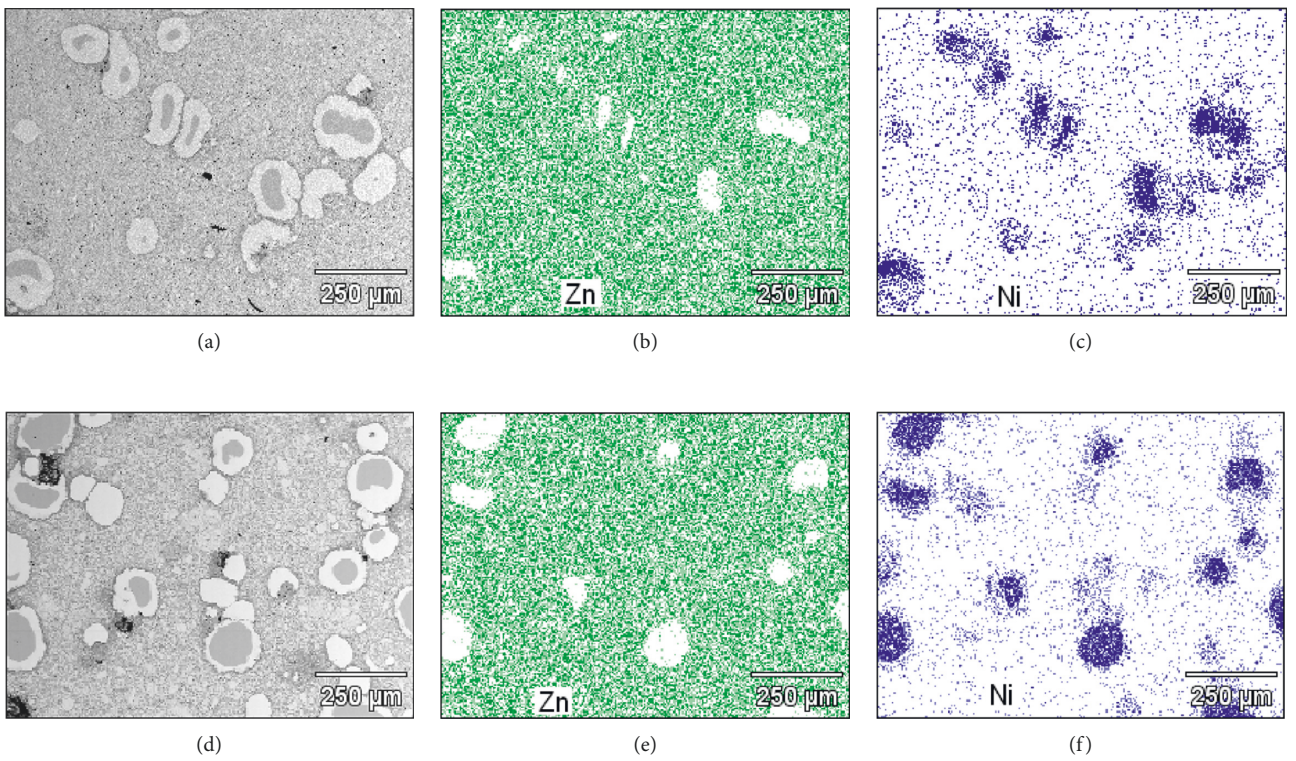

Figure 9: SEM-EDS elemental maps for the Zn-Ni_x sintered powder alloy obtained by X-ray fluorescence. (a) SEM microstructure of the Zn-Ni_5 alloy and its elemental map for Zn (b) and for Ni (c) and (d) SEM microstructure of the Zn-Ni_{10} alloy and its elemental map for Zn (e) and for Ni (f).

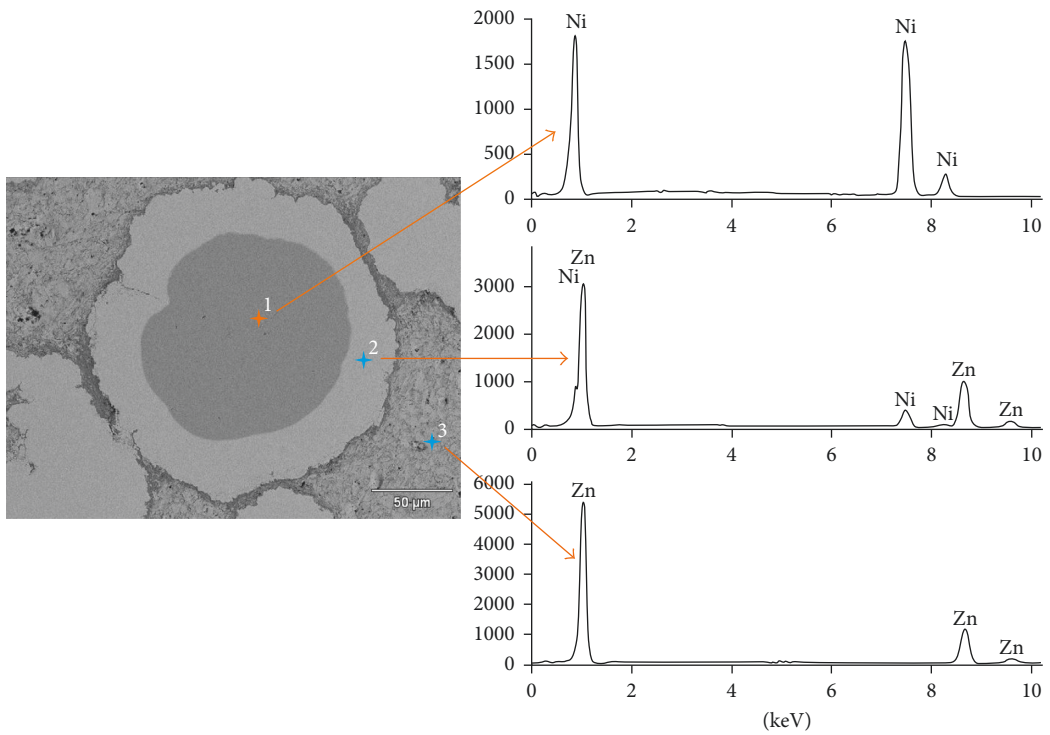

Figure 10: SEM micrograph and EDS spectra of the Zn-Ni_{10} sintered powder particle, showing different phases.

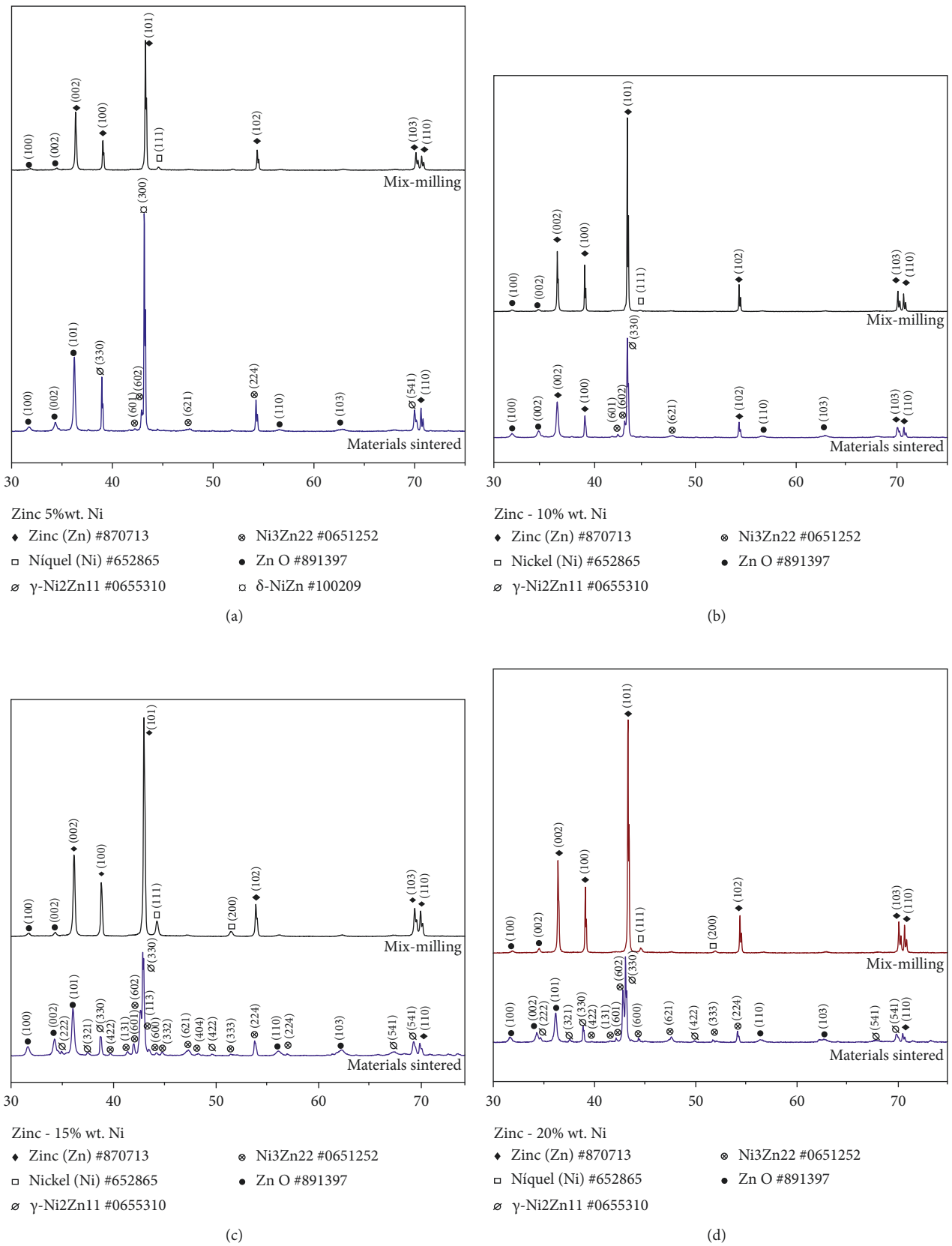

Figure 11: X-ray diffraction spectra of milling powders and sintered materials of systems Zn-Ni_x. (a) Zinc 5%wt. Ni. (b) Zinc 10%wt. Ni. (c) Zinc 15%wt. Ni. (d) Zinc 20%wt. Ni.

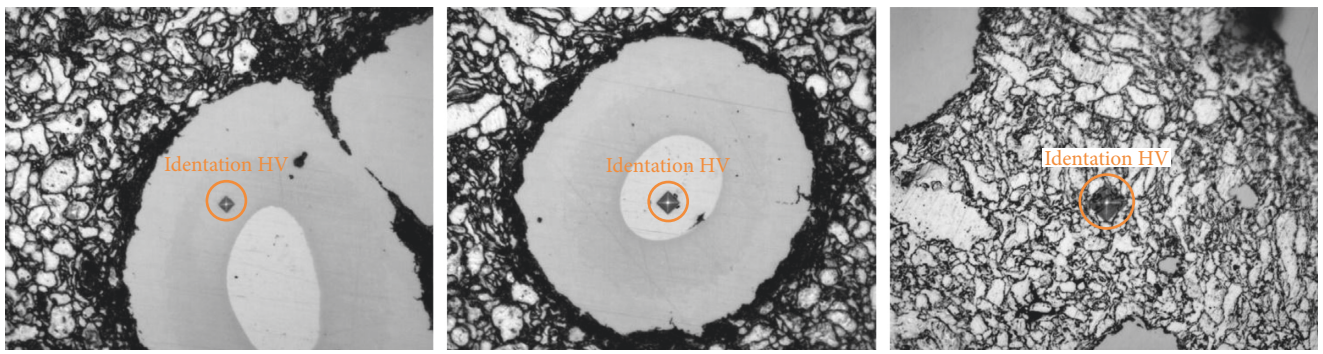

Figure 12: Vickers hardness test of the intermetallic region, showing (a) NiZn phase, (b) Ni phase, (c) Zn phase.

associated with Zn_2O phase. A decrease in Zn related to the intensities of characteristic Kα-lines after sintering can be equally associated with the oxidation phenomenon by the introduction of oxygen into the crystal lattice of Zn/Zn_2O, and oxygen causes a strong structural distortion and lattice deformation resulting in the formation of an amorphous structure. Furthermore, there is a slight decrease in the broadening of spectra lines with respect to sintered samples. This phenomenon is due to the alteration of crystal size and the reduction of internal microdeformation to the crystal lattice according to the ratio of Scherrer spectrum to the spectrum of the diffracted rays analyzed in the reciprocal space, and this size is inversely proportional to the width in the middle position with intensity relative to 2θ [37]. According to the Zn-Ni phase diagram that is shown in Figure 3, the percentage composition of the study systems ranges from $0\% < Ni < 15\%$, and an intermetallic phase δ is presented, while in the range of $15\% < Ni < 20\%$, the intermetallic phase changes to γ; however, considering that the limit of 15% can have the presence of both phases, according to this diagram, there is not any chance of possibility of finding intermetallic phases of β and β_1 [38]. It is important to note that according to the XRD spectra of the systems Zn-Ni_5, Zn-Ni_{10}, Zn-Ni_{15}, and Zn-Ni_{20} during high-energy milling, no formation of intermetallic phases was identified, whereas the main mechanism for the formation of these kinds of phases is by increasing the energy during the impact between the grinding media and powders to enable the diffusion and promote the reaction of formation of the intermetallic compound. In the particular case of these systems and due to the manufacturing methodology proposed in this research, high-energy milling is just a mix-milling process that homogenizes the composition of the systems. In this sense, some systems do not present the formation of these compounds by mechanical action due to insufficient energy transfer to the powder but obtained after a heating process [22].

In addition, the formation of Zn-Ni phases is also attributed to the Gibbs free energy [32, 36]:

$$11Zn_2 + Ni_3 \rightarrow Zn_{22}Ni_3\left(\Delta G_{530K} = -13836.48\,J \cdot mol^{-1}\right)$$
$$11Zn + Ni_2 \rightarrow Zn_{11}Ni_2\left(\Delta G_{530K} = -850.54\,J \cdot mol^{-1}\right) \quad (1)$$

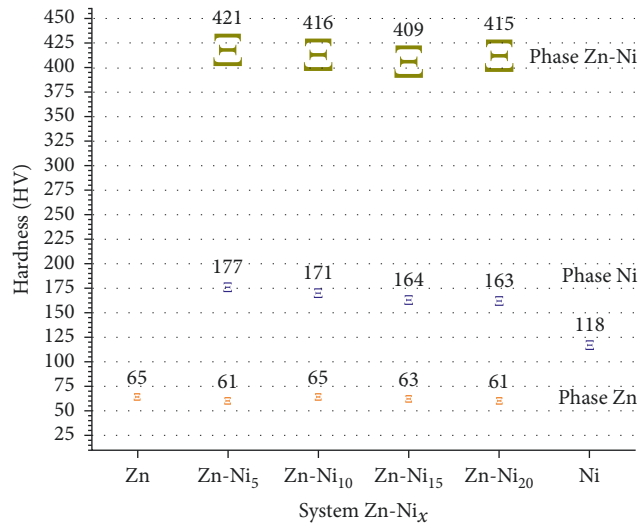

Figure 13: Zn and Ni behavior on microhardness properties of the Zn-Ni_x sintered powder alloy system.

The negative ΔG° of $Zn_{22}Ni_3$ is higher than that of the $Zn_{11}Ni_2$ phase, which indicates that the $Zn_{22}Ni_3$ phase must be formed first during heating treatment. XRD showed more peaks associated with the $Zn_{22}Ni_3$ phase compared to $Zn_{11}Ni_2$, which is consistent with the thermodynamic results described above.

3.3. Hardness. The mechanical behavior (microhardness) of the obtained compounds corresponding to the Zn-Ni_x system alloy as a function of Ni content (Zn-Ni, Zn-Ni10, Zn-Ni15, and Zn-Ni20) has in general different hardness value depending on the phase where it is measured. Figure 12 shows some typical micrographs of the Zn-Ni_{10} compound exhibiting different regions where hardness Vickers (HV) was measured; that is, indentation prints were taken on the intermetallic phase (Zn-Ni), the Ni-rich phase, and the Zn-richest zone (metallic matrix), respectively, as that shown in the optical images.

The results of the hardness can be seen in the graph in Figure 13; herein, the behavior of the hardness is observed as a not dependence function of increasing Ni wt.% content

in the metallic matrix (Zn). In this graph, the average hardness value of the reference materials (Ni or Zn in pure condition) is also present; it is worth noting that the latter material was sintered according to 85% of its melting temperature. It can be seen that the hardness of materials depends on the increase in the percentage of Ni content in the Zn-rich phase, which exhibits the following behavior that ranges from 65 HV, 61 HV, 65 HV, and 63 HV, respectively, for Zn-Ni_5, Zn-Ni_{10}, Zn-Ni_{15}, and Zn-Ni_{20} compounds with an average deviation of ±3 HV. Whereas for the Zn-Ni_{10} compound, it exhibits a typical microstructure obtained by mechanical milling that is characterized by randomly semispherical particles segregated homogeneously in the entire metallic matrix. Microstructural and EDS analyses revealed that there were three distinct phases that are present in each particle, as evident from Figures 10 and 11. The region in which Zn is in the large proportion (δ-phase), the hardness value is about 65 HV in average, but in those regions where Ni-α is segregated, the hardness increases until 168.8 HV in average; however, due to the atomic diffusion mechanism during the sintering treatment, an intermetallic compound (γ-ZnNi) is formed, and the hardness value obtained in this phase is about 416 HV with an average deviation of ±10 HV. In general, the increase in %Ni-α phases that were identified in all the compounds of the Zn-Ni_x system does not cause a remarkable increase in the microhardness since the sintering temperature and time are the same parameters in all the synthesis materials, and the thermal effect is also the same.

While having a constant average behavior of the microhardness in each phase according to the graph in Figure 13, in analogy to increase the %Ni-α in the composition, the increase in the Ni-alpha-rich phase (observed in Figure 6) is associated with the formation of intermetallic phases during the sintering process in the solid state. By increasing these phases and those having the greatest microhardness value, it may be that the hardness value of the material also increases proportionally to the increase of the number of intermetallic phases.

4. Conclusions

The manufacturing process of the Zn-Ni_x system alloy is feasible for the Zn-Ni_5, Zn-Ni_{10}, Zn-Ni_{15}, and Zn-Ni_{20} compositions by the process of mechanical milling at high energy and sintering in the solid state. Commonly, the materials obtained by a nonconventional synthesis process are innovative with unique properties and applications, according to EDS analysis. The structure is composed by intermetallic phases (γ-ZnNi) with pure Ni core that are homogenously spread out into a metallic (Zn) matrix by mechanical energy effects.

X-ray patterns suggest that intermetallic phases did not form during the ball milling because of the lower milling time (4 h); However, intermetallics appear only after the sintering process activated by the mechanics of solid-state diffusion.

The best densification was achieved at about 90.3% for the Zn-Ni_5 compound. In the other components, the density decreases when the percent of Ni content increases due to major porosity present in the material.

The increase in the percentage of Ni content in the Zn-Ni_x system alloy (Zn-Ni_5, Zn-Ni_{10}, Zn-Ni_{15}, and Zn-Ni_{20}) promotes the growth of intermetallic phases during sintering, indicative of lattice distortion of the hexagonal structure (hcp) of the Zn phase favoring the diffusion mechanism. An alteration of the fcc-cubic structure that corresponds to the Ni phase is also observed in the X-ray patterns so that the dissolution of its atoms into the Zn matrix produces the phase transformation into δ-ZnNi (intermetallic phase) at 5% of Ni, while for percentages of 10, 15, and 20% by weight of Ni, the phase was transformed into γ-ZnNi.

The microhardness properties were dependent on the phases present in Zn-Ni_5, Zn-Ni_{10}, Zn-Ni_{15}, or Zn-Ni_{20} compound. The Ni-α phase transformed into the γ-ZnNi intermetallic phase, and the microhardness value shifted from about 60 HV to 400 HV units, which makes the alloy very useful for applications at high performance.

Conflicts of Interest

The authors declare that there are no conflicts of interest.

Acknowledgments

Members of the research group of CA-Ingenieria Industrial Avanzada would like to thank the SEP for its financial support to UAEM-CA-202 project (Programa al Fortalecimiento a Cuerpos Academicos 2015 IDCA: 17591) and PFCE-SEP 2017 (financial funds) and the IPN for its technical support in the SEM micrographs obtained by EDS and XRD analyses. Finally, the authors are grateful to CONACyT for its distinction and encouragement as national researcher SNI.

References

[1] E. Said Gouda, "Classifications, characterization and applications of metallic alloys," *International Journal of Physics and Astronomy*, vol. 2, no. 2, pp. 15–49, 2014.

[2] G. Barceló, E. Garciâ, M. Sarret, C. Müller, and J. Pregonas, "Characterization of zinc-nickel alloys obtained from an industrial chloride bath," *Journal of Applied Electrochemistry*, vol. 28, no. 10, pp. 1113–1120, 1998.

[3] M. E. P. Souza, E. Ariza, M. Ballester, I. V. P. Yoshida, L. A. Rocha, and C. M. A. Freire, "Silicone resin to improve corrosion resistance of Zn and ZnFe coated steel," *Revista Matéria*, vol. 11, no. 1, pp. 16–23, 2006.

[4] G. Chen, K. D. Liss, and P. Cao, "An in situ study of NiTi powder sintering using neutron diffraction," *Metals*, vol. 5, no. 2, pp. 530–546, 2015.

[5] N. Setoudeh, M. H. Paydar, and M. Sajjadnejad, "Effect of high energy ball milling on the reduction of nickel oxide by zinc powder," *Journal of Alloys and Compounds*, vol. 623, pp. 117–120, 2015.

[6] S. Bid and S. K. Pradhan, "Characterization of crystalline structure of ball-milled nano-Ni–Zn-ferrite by Rietveld method," *Materials Chemistry and Physics*, vol. 84, no. 2-3, pp. 291–301, 2004.

[7] J. Park, W. Kim, C. Suh, and S. Kim, "Catalytic properties of Ni-Zn alloy prepared by mechanical alloying for steam reforming from methanol," *Metals and Materials International*, vol. 18, no. 2, pp. 237–241, 2012.

[8] J. M. Kim, J. S. Park, and H. S. Yun, "Microstructure and mechanical properties of TiC nanoparticle-reinforced iron-matrix composites," *Strength of Materials*, vol. 46, no. 2, pp. 177–182, 2014.

[9] K. S. Mohammed and H. T. Naeem, "Effect of milling parameters on the synthesis of Al-Ni intermetallic compound prepared by mechanical alloying," *Physics of Metals and Metallography*, vol. 116, no. 9, pp. 859–868, 2015.

[10] M. A. Ahmed, E. Ateia, L. M. Salah, and A. A. El-Gamal, "Structural and electrical studies on La^{3+} substituted Ni–Zn ferrites," *Materials Chemistry and Physics*, vol. 92, no. 2-3, pp. 310–321, 2005.

[11] G. Penev-Vassilev, T. Gomez-Acebo, and J. C. Tedenac, "Thermodynamic optimization of the Ni-Zn system," *Journal of Phase Equilibria*, vol. 21, no. 3, pp. 287–301, 2000.

[12] T. Lee, D. S. Shih, Y. Lee, and C. S. Lee, "Manufacturing ultrafine-grained Ti-6Al-4V bulk rod using multi-pass caliber-rolling," *Metals*, vol. 5, no. 2, pp. 777–789, 2015.

[13] B. Thangjam and I. Soibam, "Comparative study of structural, electrical, and magnetic behaviour of Ni-Cu-Zn nanoferrites sintered by microwave and conventional techniques," *Journal of Nanomaterials*, vol. 2017, Article ID 5756197, 10 pages, 2017.

[14] C. Stergiou, "Microstructure and electromagnetic properties of Ni-Zn-Co ferrite up to 20 GHz," *Advances in Materials Science and Engineering*, vol. 2016, Article ID 1934783, 7 pages, 2016.

[15] K. I. Chen, S. C. Cheng, C. H. Cheng, S. Wu, Y. L. Jiang, and T. C. Cheng, "The Effects of gallium additions on microstructures and thermal and mechanical properties of Sn-9Zn solder alloys," *Advances in Materials Science and Engineering*, vol. 2014, Article ID 606814, 10 pages, 2014.

[16] R. Casati and M. Vedani, "Metal matrix composites reinforced by nano-particles—a review," *Metals*, vol. 4, no. 1, pp. 65–83, 2014.

[17] I. S. El-Mahallawi, A. Y. Shash, and A. E. Amer, "Nano-reinforced Cast Al-Si Alloys with Al_2O_3, TiO_2 and ZrO_2 Nanoparticles," *Metals*, vol. 5, no. 2, pp. 802–821, 2015.

[18] J. A. Aragón, J. R. Miranda, I. Hilerio et al., "Compuestos de matriz metálica rica en Zn, con alto contenido de Al y componentes estructurales de compuestos intermetálicos de Cu-Zn y Cu-Al particulados," *Revista Mexicana de Física*, vol. 53, no. 2, pp. 105–113, 2007.

[19] V. Viswanathan, T. Laha, K. Balani, A. Agarwal, and S. Seal, "Challenges and advances in nanocomposite processing techniques," *Materials Science and Engineering: R: Reports*, vol. 54, no. 5-6, pp. 121–285, 2006.

[20] R. A. Rodríguez-Díaz, A. Sedano, A. Molina-Ocampo, J. Porcayo-Calderón, J. Uruchurtu, and M. Gonzalez-Pérez, "Producción de una aleación nanoestructurada FeAl mediante aleación mecánica y su caracterización microestructural," *Avances en Ciencias e Ingeniería*, vol. 4, no. 4, pp. 95–104, 2013.

[21] H. Kang, S. J. Lee, and I.-J. Shon, "Rapid synthesis and consolidation of nanostructured (Mo, W)Si_2 by high-frequency induction heated sintering and its mechanical properties," *Journal of Ceramic Processing Research*, vol. 15, no. 5, pp. 286–289, 2014.

[22] E. G. de Araujo, R. M. Leal-Neto, M. F. Pillis, and F. Ambrózio-Filho, "High energy ball milling processing," *Materials Science Forum*, vol. 416–418, no. 4, pp. 128–133, 2003.

[23] C. Carreño-Gallardo, I. Estrada-Guel, M. Romero-Romo, R. Cruz-García, C. López-Meléndez, and R. Martínez-Sánchez, "Characterization of Al_2O_3NP–Al_{2024} and Ag_CNP–Al_{2024} composites prepared by mechanical processing in a high-energy ball mill," *Journal of Alloys and Compounds*, vol. 536, pp. S26–S30, 2012.

[24] Ö. Balci, K. Gokuldoss-Prashanth, S. Scudino et al., "Effect of milling time and the consolidation process on the properties of Al matrix composites reinforced with Fe-based glassy particles," *Metals*, vol. 5, no. 2, pp. 669–685, 2015.

[25] W. A. Badawy, H. Nady, and G. M Abd EI-Hafez, "Electrodeposited Zn-Ni alloys as promising catalysts for hydrogen production-preparation, characterization and electrocatalytic activity," *Journal of Alloys and Compounds*, vol. 699, pp. 1146–1156, 2017.

[26] I. Herraiz-Cardona, E. Ortega, and V. Pérez-Herranz, "Impedance study of hydrogen evolution on Ni/Zn and Ni–Co/Zn stainless steel based electrodeposits," *Electrochimica Acta*, vol. 56, no. 3, pp. 1308–1315, 2011.

[27] M. J. De Giz, S. A. S. Machado, L. A. Avaca, and E. R. Gonzalez, "High area Ni-Zn and Ni-Co-Zn codeposits as hydrogen electrodes in alkaline solutions," *Journal of Applied Electrochemistry*, vol. 22, no. 10, pp. 973–977, 1992.

[28] J. Divised, H. Schmitz, and J. Balej, "Ni and Mo coatings as hydrogen cathodes," *Journal of Applied Electrochemistry*, vol. 19, no. 4, pp. 519–530, 1989.

[29] T. Hussain, M. T. Zubaida Butt, M. N. Ahmed et al., "Fabrication of Ag and Ni nanocatalyst, with enhanced efficiency," *Journal of Chemistry*, vol. 2015, Article ID 601484, 4 pages, 2015.

[30] F. Meng, P. Zhong, Z. Li, X. Cui, and H. Zheng, "Surface structure and catalytic performance of Ni-Fe catalyst for low-temperature CO hydrogenation," *Journal of Chemistry*, vol. 2014, Article ID 534842, 7 pages, 2014.

[31] J. N. Rivera Olvera, G. J. Gutiérrez Paredes, A. Romero Serrano et al., "Synthesis and characterization of a MoWC-WC-NiC nanocomposite via mechanical alloying and sintering," *Powder Technology*, vol. 271, pp. 292–300, 2015.

[32] J. N. Rivera-Olvera, J. Acevedo-Martínez, H. Herrera-Hernández, I. García-Orozco, and L. Díaz-Barriga-Arceo, "Microstructural characterization and thermodynamic analysis of MoZn produced by mechanical alloying," *Journal of Alloys and Compounds*, vol. 696, pp. 329–337, 2007.

[33] X. Su, N. Y. Tang, and J. M. Toguri, "Thermodynamic assessment of the Ni-Zn system," *Journal of Phase Equilibra*, vol. 23, no. 2, pp. 140–148, 2002.

[34] P. Li, T. Chen, S. Zhang, and R. Guan, "Research on semisolid microstructural evolution of 2024 aluminum alloy prepared by powder thixoforming," *Metals*, vol. 5, no. 2, pp. 547–564, 2015.

[35] J. A. Aragón and J. R. Miranda, "Materiales compuestos de matriz metálica rica en Zn con alto contenido de Al y componente estructural de ZnO," *Revista Mexicana de Física*, vol. 51, no. 4, pp. 356–364, 2005.

[36] W. Xiong, H. Xu, and Y. Du, "Thermodynamic investigation of the galvanizing systems, II: thermodynamic evaluation of the Ni–Zn system," *Calphad*, vol. 35, no. 3, pp. 276–283, 2011.

[37] B. D. Cullity, "Elements of X-Ray Diffraction," *Series in Metallurgy and Materials*, Addison-Wesley, Boston, MA, USA, 2nd edition, 1977.

[38] P. Nash and Y. Y. Pan, *Phase Diagrams of Binary Nickel Alloys*, P. Nash, Ed., pp. 382–390, ASM International, Materials Park, OH, USA, 1991.